Supporting Information for "The Seasonal Cycle of Significant Wave Height in the Ocean: Local vs Remote Forcing"

Luke Colosi[1], Ana B. Villas Bôas[1], Sarah T. Gille[1]

[1]Scripps Institution of Oceanography, La Jolla, California

Contents of this file

1. Figures S1 to S9

Introduction

Here we present nine additional figures along with discussion about methods for computing decorrelation time scales to support the results in the main text. Figure S1 explores the wave shadowing by the Polynesian islands. Figure S2 shows fractional uncertainty of amplitude for annual and semi-annual cycles to illustrate the geographic location of high fractional uncertainty regions. Figure S3 examines other Seasonal Wind Anomaly Region (SWAR) definition criteria to show how highlighted regions in Figure 3 of main text change as the SWAR criteria become more restrictive. Figure S4 explores the basin-scale SWH and WSP climatologies along with their annual cycle to illustrate the relationship between basin-averaged wind and waves. Figures S5, S6, and S7 investigates the regional

---

Corresponding author: L. V. Colosi, Scripps Institution of Oceanography, University of California San Diego, La Jolla, CA, USA. (lcolosi@ucsd.edu)

January 20, 2021, 12:09am

climatologies of SWARs not analyzed in the main text to further illustrate the unique significant wave height (SWH) variability of each SWAR based on regional and wave field characteristics. Figures S8, S9 explores model parameters of the Climate Forecast System Reanalysis (CFSR) wind speed (WSP) and WAVE-height, WATer depth and Current Hindcasting III (WW3) SWH to show similarities and differences to the Cross Calibrated Multi-Platform version 2 (CCMP2) WSP and the Institut français de recherche pour l'exploitation de la mer (IFREMER) SWH.

January 20, 2021, 12:09am

1. Decorrelation Time Scales for IFREMER, CCMP2, and WW3

Decorrelation time scales over each month of the CCMP2 WSP, IFREMER SWH and WW3 WSP and SWH daily data are computed employing an integral time scale method used by Gille (2005). The unbiased estimator of the autocorrelation function C(n), defined at the nth lag as:

$$C(n) = \frac{\frac{1}{N-n}\sum_{i=1}^{N-n}(x_i - \bar{x})(x_{i+n} - \bar{x})}{\frac{1}{N}\sum_{i=1}^{N}(x_i - \bar{x})^2}, \tag{1}$$

was computed over the monthly segments for positive and negative lag. In (1), x_i is the ith data point in a month time series. Monthly segments of wind and wave data were detrended before computing the autocorrelation function. To compute the decorrelation time scale τ, the unbiased autocorrelation function is integrated:

$$\tau = \sum_{n=-l}^{l}\left[1 - \frac{|n|}{l}\right]C(n)\Delta t \tag{2}$$

where Δt is the separation between observations and $l \leq N$. Here, we vary l in the summation from 0 to N and take the maximum decorrelation time scale as our best estimate of τ. Decorrelation time scale data for monthly segments of CCMP2 WSP, IFREMER SWH and WW3 WSP and SWH daily data can be found at the University of California, San Diego library data repository (doi will be provided upon acceptance).

2. Island Shadowing in Equatorial Pacific

Figure S1A shows the enlarged map of SWH annual cycle phase in the Polynesian island region. Black edged boxes highlight regions where island shadowing occurs. On the Northward facing coast of islands within boxes, waves are in phase with the Northern Hemisphere annual cycle. Figure S1B shows the enlarged map of probability of swell in austral winter from Figure 8 of the main text in the same region as Figure S1A. Probability

January 20, 2021, 12:09am

of swell is low compared to surrounding regions in the boxed regions in Figure S1A. This suggests that the wave field is dominated by wind seas a higher percentage of time than surrounding regions during austral summer and thus swell originating in the higher latitudes of the Southern Hemisphere is blocked by islands. The swell able to reach the Northward facing shore comes from predominately the Northern Hemisphere causing the phase to align with the North Hemisphere annual cycle.

3. Fractional Uncertainty of IFREMER and CCMP2 Amplitude Model Parameters

Figure S2 shows the fractional uncertainty of IFREMER and CCMP2 amplitude model parameters used to determine statistical significance of amplitude and phase. Let A be the amplitude estimate for the annual or semi-annual cycle computed from the weighted least-squares fit and δA be its uncertainty, defined as the standard error, computed by propagating errors. Estimate A and its corresponding phase ϕ are considered not statistically significant if:

$$\frac{\delta A}{A} \geq \frac{1}{2} \tag{3}$$

That is, estimates of the amplitude that are less than or equal to two standard errors are not statistically different from zero. The fractional uncertainty is greater than $1/2$ primarily in regions with near zero amplitude for SWH and WSP annual and semi-annual cycles.

4. Varying SWAR Criteria Threshold

Figure S3 shows maps of the annual cycle phase of CCMP2 WSP highlighting SWARs using three different criteria: Figure S3A uses the same criterion as Figure 3 in the

January 20, 2021, 12:09am

main text, Figure S3B highlights regions with a WSP maximum occurring from May through September for the Northern Hemisphere, and from November through March for the Southern Hemisphere, and Figure S3C highlights regions with a WSP maximum occurring from June through August for the Northern Hemisphere, and from December through February for the Southern Hemisphere. In Figure S3A-C, criteria are labeled as least, moderately and most restrictive. Comparing Figures S3A and S3C, Northern Hemisphere SWARs with the exception of the Western Mexican Coast and Hawaii are not present when the criteria become more restrictive. This suggests Northern Hemisphere SWARs tend to have WSP annual cycle maxima during late spring or early fall months. The $15°$ to $30°$ zonal band of Southern Hemisphere SWARs significantly reduces to only coastal regions when the criteria become more restrictive. The percent of the global ocean surface from $-66°$ to $66°$ latitude experiencing anomalous winds is 3.39%, 1.28%, and 0.66% respectively for Figures S3A, S3B, and S3C criteria.

5. Basin-Scale Monthly Climatologies

Figure S4 shows the SWH (solid blue) and WSP (solid red) monthly climatologies for North and South Pacific and Atlantic and Indian Ocean basins along with SWH (dashed blue) and WSP (dashed red) annual cycles. SWH and WSP basin-scale climatologies in all SWARs, except for the Indian Ocean, predominately exhibit annual cycles variability with nearly identical phase. Fraction of variance explained by the mean and annual cycle in these SWARs for SWH and WSP range from 92% to 100%. For the Indian Ocean, SWH and WSP display annual cycle variability. However, WSP has a local maximum during austral summer. Consequentially, the fraction of variance explained by mean and annual cycle is 67% and 87% for WSP and SWH respectively. If the basin-scale climatology is

January 20, 2021, 12:09am

computed without SWH or WSP monthly climatologies above the equator in the Indian Ocean, the resulting climatology (not shown) has a significantly smaller austral summer local maximum with 87% of variance explained for WSP. This suggests that this WSP local maximum is a signature of monsoons in the Northern Indian Ocean.

6. Regional Climatologies of SWARs in Non-hypothesized Expansion Fan wind Regions

Figures S6 and S7 show regional climatologies for SWARs not included in Figures 6 and 7 in main text. Off the West Mexican coast in Figure. S6B and E and East Australian coast in Figure S7F and L, the WSP and SWH climatologies are in phase suggesting that local wind events dominate the wave field. Furthermore, the residual between the SWH Climatology and ocean basin annual cycle in these SWARs has annual cycle structure suggesting the timing of basin-scale annual cycle is not aligned with the SWH regional climatology annual cycle. Similar to Northern Hemisphere SWARs in potential expansion fan wind regions, the Hawaiian (Figure S6A,D) and Central North Atlantic (Figure S6C,F) SWARs have a sharp summer peak in the WSP climatology coinciding with a deviation in SWH climatology from the basin-scale annual cycle. Similar to Southern Hemisphere SWARs in potential expansion fan wind regions, the Central South African coast (Figure S7A,G), the Central West Atlantic (Figure S7B,H), the Southern Mozambique Channel (Figure S7B,H), and the Central South Pacific (Figure S7D,J) have small magnitude deviations of SWH corresponding to broad peaks in the WSP Climatologies. The North Indian ocean SWAR (Figure S7E,K) has a SWH climatology that follows very closely to the basin-scale annual cycle and a WSP climatology with small peaks during October and June. This suggests the SWAR region is outside of the monsoon region and

the wave field is predominately set by remotely generated wave from the high latitude Southern Hemisphere storms.

7. Evaluation of WW3 model with CFSR wind forcing

Figure S8 shows the phasing and amplitudes of the SWH and WSP annual and semi-annual cycles for WW3 hindcast forced by CFSR winds. Except for slight differences with respect to the swell front region of the pacific and Atlantic in Figure 2A and regions considered not statistically significant, the WW3 hindcast reproduces well the model parameters in Figure 2 of the main text. Figure S9 shows the monthly climatologies of IFREMER SWH, CCMP2 WSP, CFSR WSP, and WW3 SWH in the same potential expansion fan regions as in Figures 5,6. All three data sets reproduce the same seasonal variability despite CFSR WSP's slight overestimate bias.
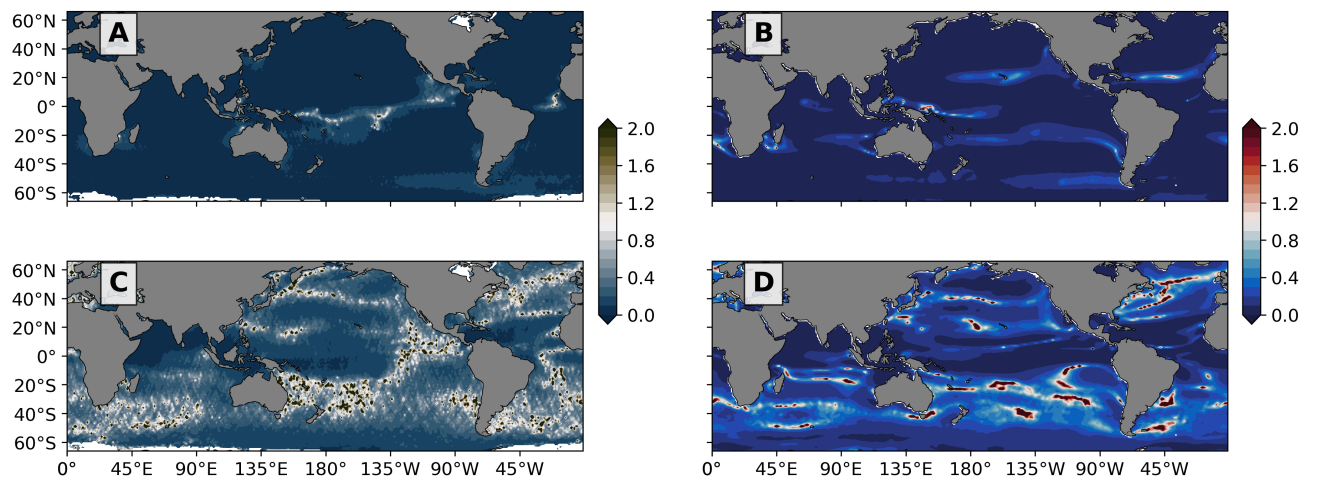
January 20, 2021, 12:09am

Figure S1.   (A) Ifremer SWH annual cycle phase map and (B) June through August seasonal probability of swell in Polynesian island region illustrating island shadowing.

January 20, 2021, 12:09am

Figure S2. Fractional uncertainty of amplitude of annual cycle for (A) IFREMER SWH and (B) CCMP2 WSP; amplitude of semi-annual cycle for (C) IFREMER SWH and (D) CCMP2 WSP.
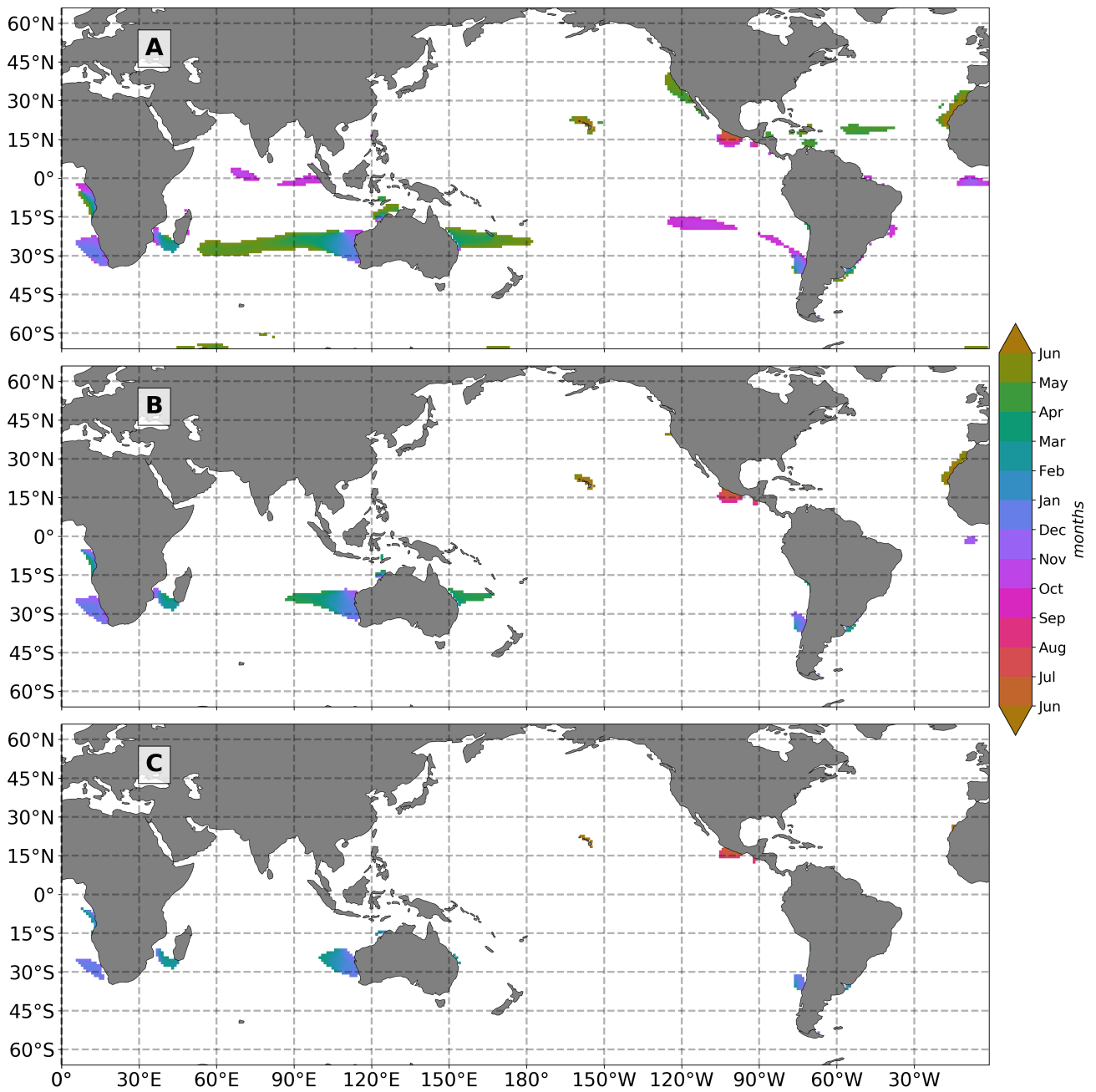
Figure S3. Maps of the annual cycle phase of CCMP2 wind speed highlighting SWARs using three different criteria: (A) least restrictive, (B) moderately restrictive, and (C) most restrictive. White pixels correspond to points that are not categorized as anomalous phase or not statistically significant.
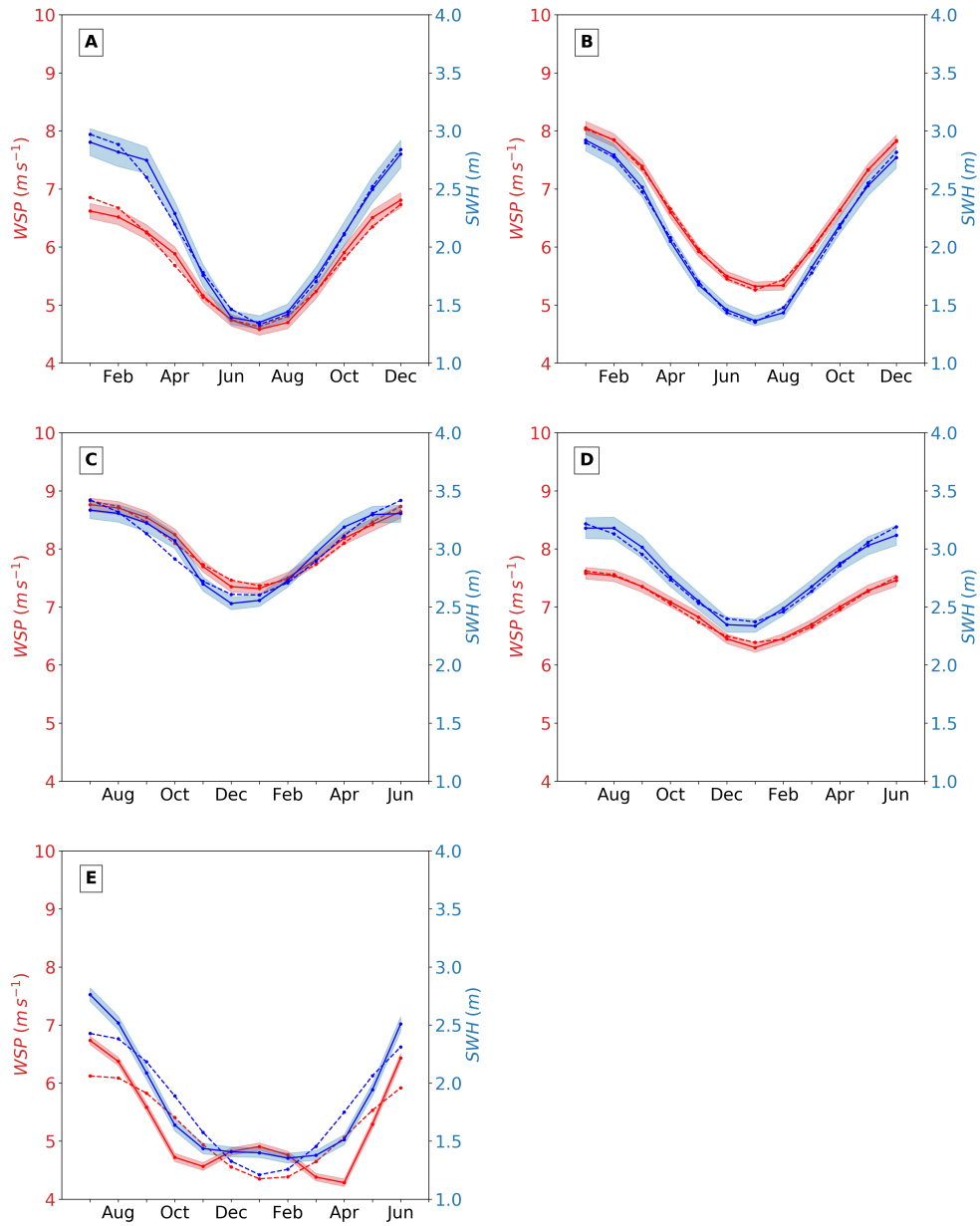
January 20, 2021, 12:09am

Figure S4. Basin-scale climatologies with Ifremer SWH (Solid blue) and CCMP2 WSP(Solid red). Blue shading represents the standard error of the mean. Dotted blue is the annual cycle weighted least-squares fitted to monthly climatology for mean SWH of the hemisphere ocean basin. Basins include (A) North Pacific, (B) North Atlantic, (C) South Pacific, (D) South Atlantic, and (E) Indian Ocean where marginal seas and the equatorial regions across the Pacific and Atlantic oceans not considered.
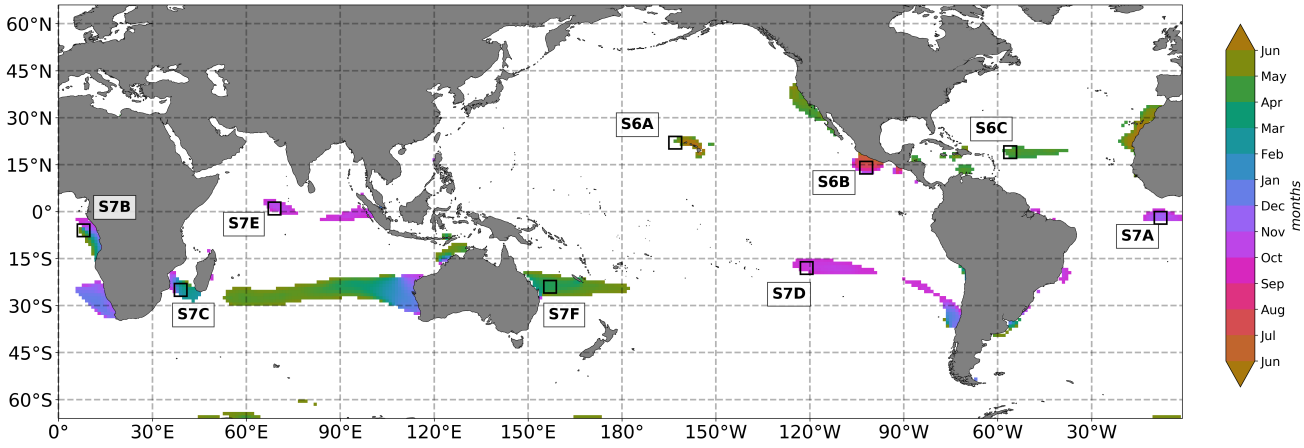
Figure S5. Same as Figure 4 from main text with geographic locations of regional climatologies

for SWARs in Figures S6, S7
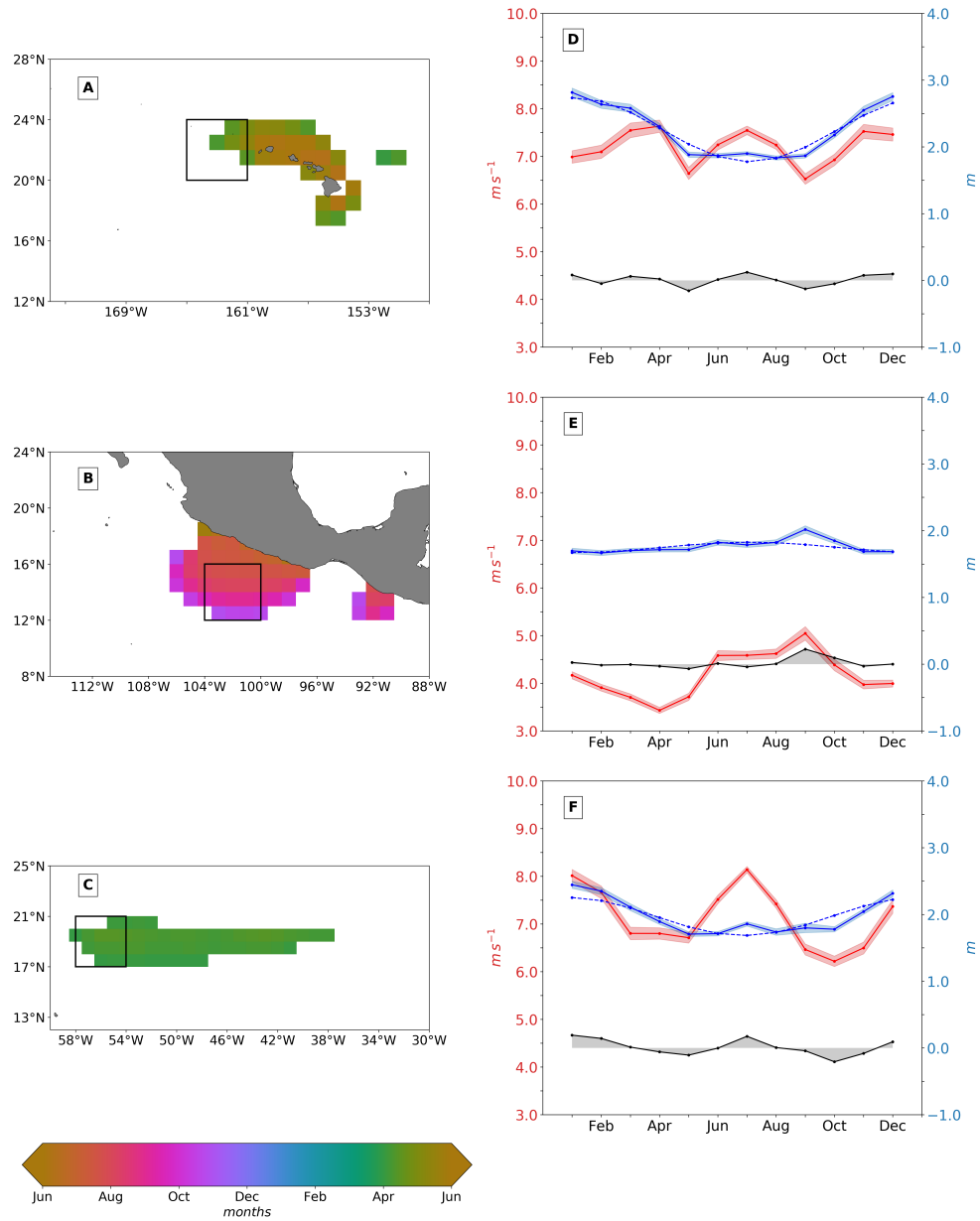
January 20, 2021, 12:09am

Figure S6.   (left column) Northern Hemisphere highlighted SWARs in Figure S5 with (right column) IFREMER SWH (solid blue) and CCMP2 WSP (solid red) climatologies extracted from the outlined 4° by 4° boxes within SWARs. Blue shading represents the standard error of the mean, dotted blue is the annual cycle weighted least-squares fitted to monthly climatology for mean SWH of the hemisphere ocean basin the SWAR is located in, and black solid is the residual between SWH regional climatology and annual cycle. SWARs include Hawaii (A and D), Western Mexican Coast (B and E), and Central North Atlantic east of Antilles Islands (C and F).
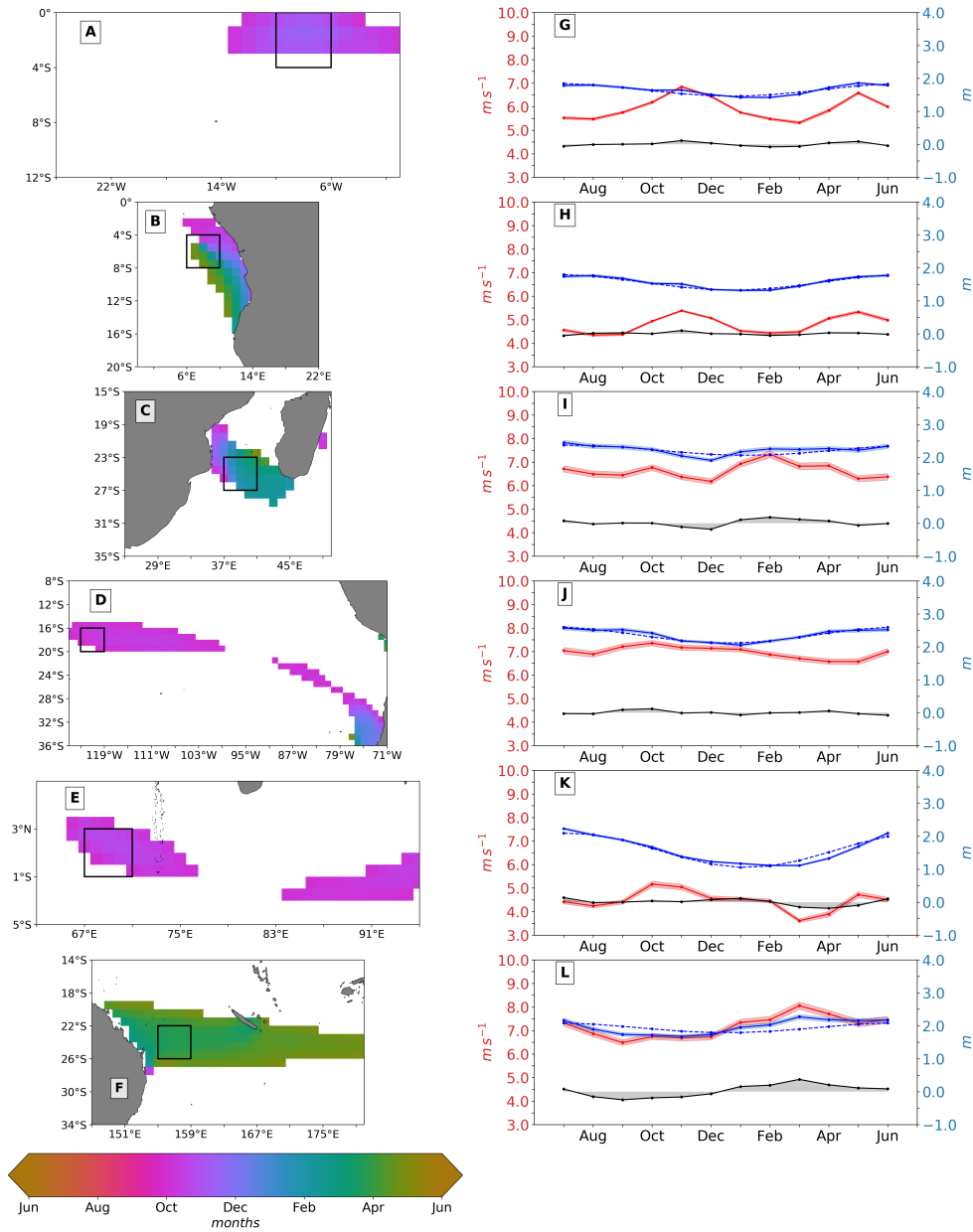
Figure S7. (left column) Southern Hemisphere highlighted SWARs in Figure S5 with (right column) IFREMER SWH (solid blue) and CCMP2 WSP (solid red) climatologies extracted from the outlined 4° by 4° boxes within SWARs. Shading, dotted lines, and solid black are as in Figure S6. SWARs include Central South Atlantic Ocean (A and G), Central West coast of Africa (B and H), Southern Mozambique Channel (C and I), mid-latitude Southern Pacific (D and J), North Indian Ocean (E and K), and Eastern Australian coast. (F and L).
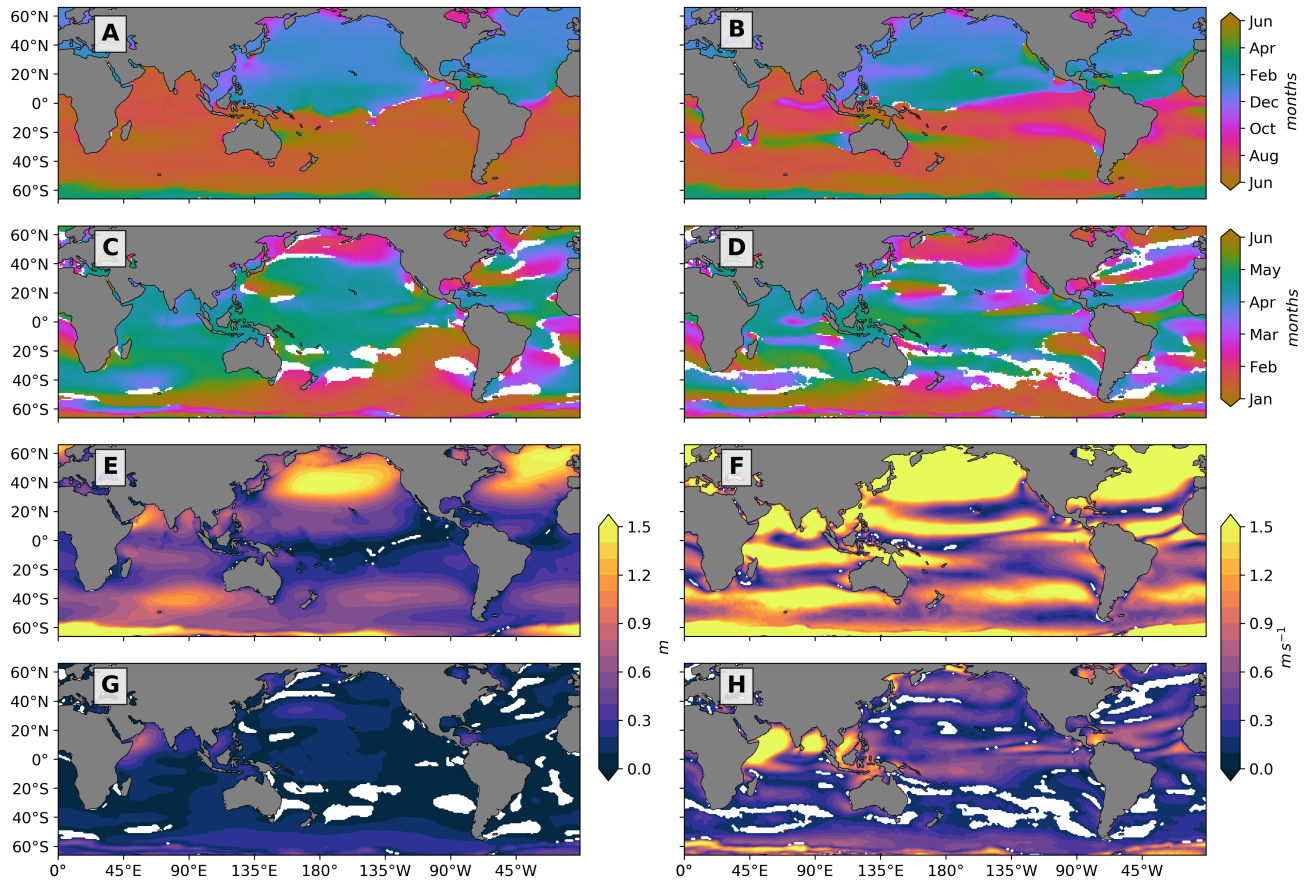
January 20, 2021, 12:09am

Figure S8. Phase of annual cycle for (A) WW3 SWH and (B) CFSR WSP; phase of semi-annual cycle for (C) WW3 SWH and (D) CFSR WSP; amplitude of annual cycle for (E) WW3 SWH and (F) CFSR WSP; amplitude of semi-annual cycle for (G) WW3 SWH and (H) CFSR WSP. Grid points with a amplitude less than or equal to 2 standard deviations are considered not statistically significant and masked white; the same pixels are also masked for phase. See section 2.3 for details of computation.
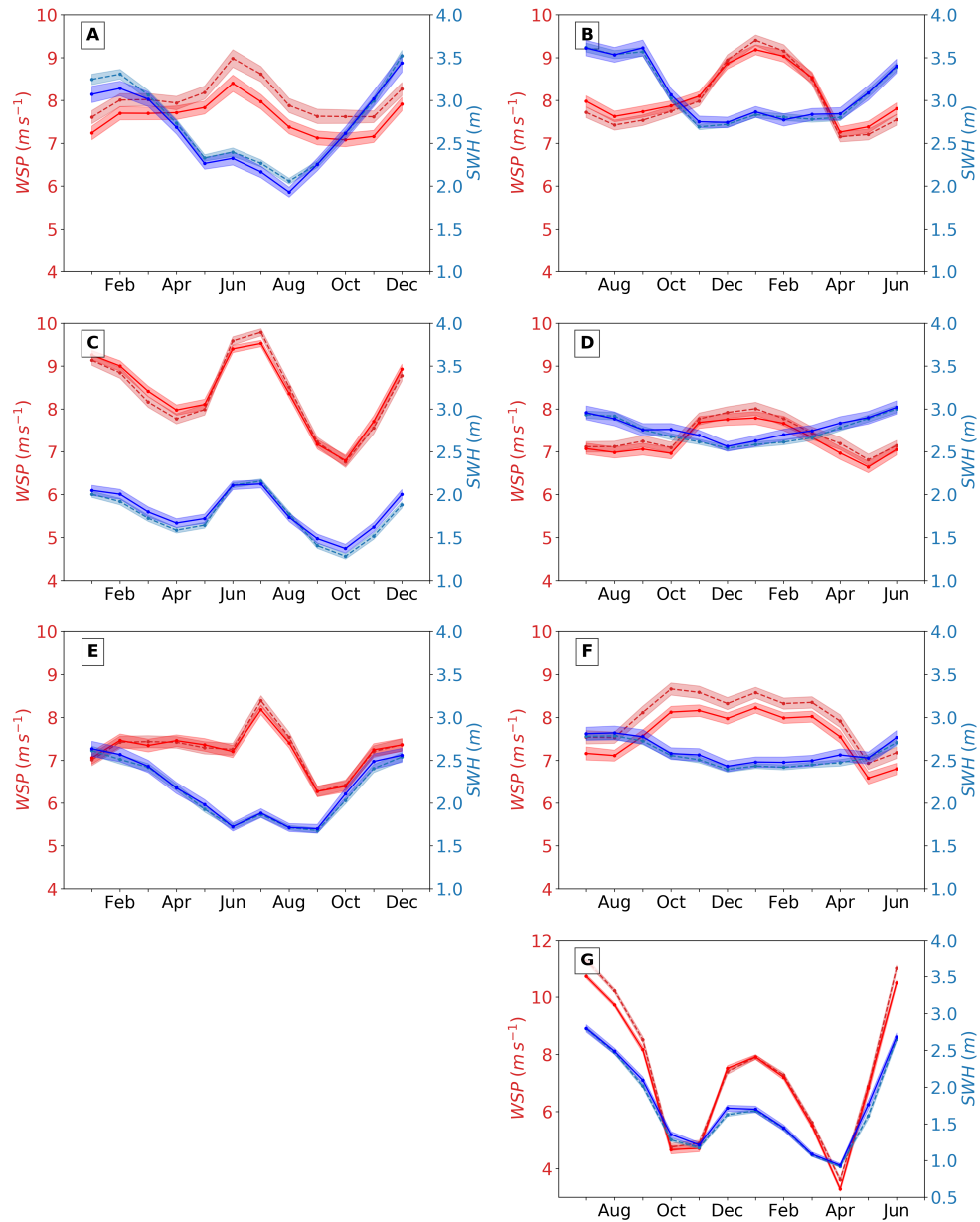
January 20, 2021, 12:09am

Figure S9.   Regional climatologies with Ifremer SWH (Solid blue), CCMP2 (Solid red), WW3

SWH (dashed blue), and WW3 WSP (dashed red). Same regions as in Figure 7.

References

Gille, S. T. (2005). Statistical characterization of zonal and meridional ocean wind stress. *Journal of Atmospheric and Oceanic Technology*, *22*(9), 1353–1372. doi: 10.1175/JTECH1789.1

January 20, 2021, 12:09am